DOI: 10.1007/s12541-014-0404-z

Second-Order Sliding Mode Control of a 3D Overhead Crane with Uncertain System Parameters

Le Anh Tuan[1], Jae-Jun Kim[2], Soon-Geul Lee[3,#], Tae-Gyoon Lim[4], and Luong Cong Nho[5]

1 Department of Mechanical Engineering, Vietnam Maritime University, Hai Phong, Vietnam
2 Graduate School of Mechanical Engineering, Kyung Hee University, 1 Seocheon-dong, Giheung-gu, Yongin-si, Gyeonggi-do 449-701, South Korea
3 School of Mechanical Engineering, Kyung Hee University, 1 Seocheon-dong, Giheung-gu, Yongin-si, Gyeonggi-do 449-701, South Korea
4 System Solution Research Department, Research Institute of Industrial Science and Technology, Pohang, Gyeongsangbuk-do 790-330, South Korea
5 Vietnam Maritime University, Hai Phong, Vietnam
Corresponding Author / E-mail: sglee@khu.ac.kr, TEL: +82-31-2012506, FAX: +82-31-2021204

KEYWORDS: Lyapunov function, 3D overhead crane, Sliding mode control, Uncertain parameters

This paper proposes a second-order sliding mode controller for a three-dimensional overhead crane in an extremely complicated operation with uncertain system parameters. Three actuators composed of trolley-moving, bridge-traveling, and cargo-hoisting forces simultaneously drive fine outputs comprising bridge motion, trolley translation, cable length, and two payload swing angles. Simulation and experiment are performed to investigate the controller qualities. The proposed controller asymptotically stabilizes and consistently maintains system response even when some system parameters are extensively varied.

Manuscript received: October 8, 2013 / Revised: February 11, 2014 / Accepted: March 3, 2014

NOMENCLATURE

m_c = cargo mass (kg)
m_t = trolley mass (kg)
m_b = lumped mass of bridge (kg)
m_l = equivalent mass of all rotating components of hoist (kg)
x = trolley displacement (m)
l = cargo suspended cable length (m)
θ and φ = cargo swing angles (rad)
u_t = trolley-traveling force (N)
u_b = bridge-moving force (N)
u_l = cargo-lifting force (N)

1. Introduction

Overhead cranes are extensively used for lifting and carrying payloads in industrial factories. Modern overhead cranes are usually operated at high speed to increase productivity. The fast motion of cranes without controls leads to large cargo swings, which cause inaccurate motions of crane mechanisms and lead to dangerous situations in operation zones.

Crane control studies have elicited considerable attention. Several papers that applied various types of control techniques have been published. Sakawa[1] and Sawodny[2] designed linear control laws by the pole placement method. Giua[3] suggested a state feedback controller and an observer based on a parameter-varying linear crane model.

Several studies have used optimal methods to examine crane control. Sakawa[4] computed the optimal algorithm to minimize payload swing and track trolley. Auernig[5] solved time optimal-control problems using Pontryagin's maximum principle. Garni[6] studied an optimized nonlinear feedback controller that satisfies specified boundary conditions and functional constraints. Wang[7] recommended an optimal asymptotic linear quadratic controller with fixed gains during payload mass variation.

Nonlinear control techniques, such as feedback linearization[8-11] and Lyapunov-based methods,[12-16] have been extensively applied in crane control design. Lee[17] proposed a Lyapunov-based controller comprising feedforward and nonlinear proportional-integral-derivative control components. Lee also designed motion-planning schemes for a two-dimensional (2D) motion cranes[18] and three-dimensional (3D) crane systems[19] that are effective in high payload-lifting speeds.

Crane control adaptive trends have also been mentioned in several papers. Hua[20] discussed a nonlinear control scheme that incorporates a

© KSPE and Springer 2014

parameter-estimating mechanism using self-turning methods. Yang[21] enhanced Hua's adaptive controller[20] for a 3D overhead crane. Teo[22] addressed another adaptive control law to control the motion of the overall gantry system without considering cargo anti-swing control. Cho[23] proposed an adaptive controller consisting of nominal proportional-derivative and corrective control components. Sun[24] applied the iterative learning strategy to design a kinematic coupling-based trajectory controller. Omar,[25] Giua,[26] and Corriga[27] applied the gain-scheduling approach to control tower and gantry cranes. Mizumoto[28] designed a multi-rate adaptive output feedback controller for a digital crane system. Ngo[29] provided an adaptive structure using boundary control for a container crane based on a distributed mathematical model.

Sliding mode control (SMC) is a well-known robust technique extensively applied in nonlinear systems. SMC general theory for a class of under-actuated systems was introduced by Lee,[30] developed by Ashrafiuon,[31] and completed by Sankaranarayanan.[32] Subsequently, a series of control crane papers that use SMC was published. Karkoub[33] introduced a variable crane system structure controller in conjunction with a state feedback control scheme and a μ-synthesis control scheme. Two overhead crane SMC schemes, a PI-based controller and a linear observer-based time-varying feedback scheme, were constructed by Bartolini.[34] Ngo[35] discussed a payload sliding mode controller for container crane anti-sway and only showed the simulation result. Bartolini[36] proposed a second-order sliding mode controller for 2D overhead crane with constant cable length. However, the payload swing response of the article clearly indicated chattering. Lee[37] calculated a first-order sliding mode controller to control the cargo swing and trolley motion concurrently. This controller was derived from sliding surface stability analysis. The sliding surface was defined by linearly combining all state errors. Almutrairi[38] enhanced Lee's study[37] and designed a first-order SMC scheme for a 3D crane system, wherein only the simulation result was included.

The present study proposes a second-order sliding mode controller for a 3D overhead crane with varied cable lengths by improving and upgrading the controllers found in earlier articles.[36,38] A real-time experimental study is included.

This paper is organized as follows. Section 2 describes a nonlinear mathematical model of a 3D overhead crane. Section 3 discusses the design of a second-order sliding mode controller comprising a scheme design and a system stability analysis. Section 4 presents the simulation and experiment. Section 5 gives the concluding remarks.

2. System Dynamics

The dynamic system (Fig. 1) comprises four masses: m_t, m_b, m_l, and m_c. The distributed masses of a bridge are converted into a lumped mass m_b set in the bridge center. The equivalent masses of hoist, trolley, and cargo are represented by m_l, m_t, and m_c, respectively. The system involves five degrees of freedom corresponding to five generalized coordinates; $x(t)$ for trolley displacement, $z(t)$ for bridge motion, and $\{l(t), q(t), j(t)\}$ are the three generalized coordinates that determine cargo position. The inner friction of wipe rope is considered a linear damping element b_r. The frictions of trolley and bridge motions are

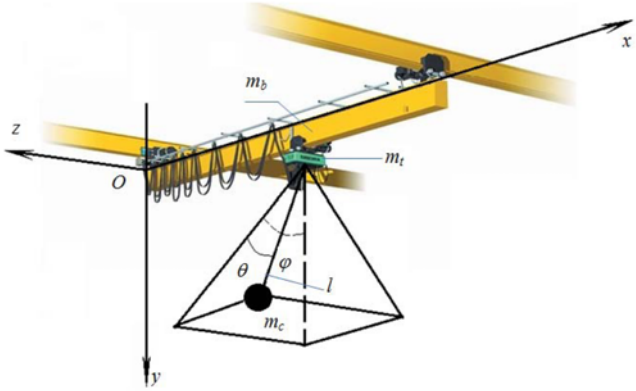

Fig. 1 Physical modeling of a 3D overhead crane

characterized by b_t and b_b respectively. The control signals u_b, u_t, and u_l denote the driving forces of trolley motion, bridge translation, and cargo hoist, respectively.

Based on the virtual power principle and Lagrange's equation, the fully nonlinear dynamics of the crane system is obtained as follows:

$$\begin{pmatrix} (m_t+m_b+m_c)\ddot{z}+m_c sin\varphi cos\theta\ddot{l}+m_c l cos\varphi cos\theta\ddot{\varphi} \\ -m_c l sin\varphi sin\theta\ddot{\theta}+b_b\dot{z}+2m_c cos\varphi cos\theta\dot{l}\dot{\varphi} \\ -2m_c sin\varphi sin\theta\dot{l}\dot{\theta}-2m_c l cos\varphi sin\theta\dot{\varphi}\dot{\theta} \\ -m_c l sin\varphi cos\theta\dot{\varphi}^2-m_c l sin\varphi cos\theta\dot{\theta}^2 \end{pmatrix} = u_b\,, \tag{1}$$

$$\begin{pmatrix} (m_t+m_c)\ddot{x}+m_c sin\theta\ddot{l}+m_c l cos\theta\ddot{\theta} \\ +b_r\dot{x}+2m_c cos\theta\dot{l}\dot{\theta}-m_c l sin\theta\dot{\theta}^2 \end{pmatrix} = u_t\,, \tag{2}$$

$$\begin{pmatrix} (m_l+m_c)\ddot{l}+m_c sin\theta\ddot{x}+m_c sin\varphi cos\theta\ddot{z} \\ +b_r\dot{l}-m_c l\dot{\theta}^2-m_c l cos^2\theta\dot{\varphi}^2-m_c g cos\varphi cos\theta \end{pmatrix} = u_t\,, \tag{3}$$

$$\begin{pmatrix} m_c l cos\varphi cos\theta\ddot{z}+m_c l^2 cos^2\theta\ddot{\varphi} \\ +2m_c l cos^2\theta\dot{l}\dot{\varphi}-2m_c l^2 cos\theta sin\theta\dot{\varphi}\dot{\theta}+m_c g l sin\varphi cos\theta \end{pmatrix} = 0\,, \tag{4}$$

$$\begin{pmatrix} m_c l cos\theta\ddot{x}-m_c l sin\varphi sin\theta\ddot{z}+m_c l^2\ddot{\theta} \\ +2m_c l\dot{l}\dot{\theta}+m_c l^2 cos\theta sin\theta\dot{\varphi}^2+m_c g l cos\varphi sin\theta \end{pmatrix} = 0\,, \tag{5}$$

These ordinary differential equations can be rewritten in matrix form as follows:

$$\mathbf{M(q)\ddot{q}+B\dot{q}+C(q,\dot{q})\dot{q}+G(q)=F}\,, \tag{6}$$

where $\mathbf{M(q)=M^T(q)}$ is a symmetric mass matrix, $\mathbf{B}$ is a damping coefficient matrix, $\mathbf{C(q,\dot{q})}$ is a Coriolis and centrifugal matrix, $\mathbf{G(q)}$ denotes a gravity vector, and $\mathbf{F}$ denotes the control forces. The components of Eq. (6) are determined by the following formulas:

$$\mathbf{M(q)}=\begin{bmatrix} m_{11} & 0 & m_{13} & m_{14} & m_{15} \\ 0 & m_{22} & m_{23} & 0 & m_{25} \\ m_{31} & m_{32} & m_{33} & 0 & 0 \\ m_{41} & 0 & 0 & m_{44} & 0 \\ m_{51} & m_{52} & 0 & 0 & m_{55} \end{bmatrix},\ \mathbf{B}=\begin{bmatrix} b_b & 0 & 0 & 0 & 0 \\ 0 & b_t & 0 & 0 & 0 \\ 0 & 0 & b_r & 0 & 0 \\ 0 & 0 & 0 & 0 & 0 \\ 0 & 0 & 0 & 0 & 0 \end{bmatrix},$$

$$\mathbf{q}=\begin{bmatrix} z \\ x \\ l \\ \varphi \\ \theta \end{bmatrix},\ \mathbf{C}(\mathbf{q},\dot{\mathbf{q}})=\begin{bmatrix} 0 & 0 & c_{13} & c_{14} & c_{15} \\ 0 & 0 & c_{23} & 0 & c_{25} \\ 0 & 0 & 0 & c_{34} & c_{35} \\ 0 & 0 & c_{43} & c_{44} & c_{45} \\ 0 & 0 & c_{53} & c_{54} & c_{55} \end{bmatrix},\ \mathbf{G}(\mathbf{q})=\begin{bmatrix} 0 \\ 0 \\ g_3 \\ g_4 \\ g_5 \end{bmatrix},\ \mathbf{F}=\begin{bmatrix} u_b \\ u_t \\ u_l \\ 0 \\ 0 \end{bmatrix}.$$

The coefficients of the $\mathbf{M}(\mathbf{q})$ matrix are determined by the following equations:

$$m_{11}=m_t+m_b+m_c,\ \ m_{13}=m_{31}=m_c sin\varphi cos\theta,$$

$$m_{14}=m_{41}=m_c l cos\varphi cos\theta,\ \ m_{15}=m_{51}=-m_c l sin\varphi sin\theta,$$

$$m_{22}=m_t+m_c,\ \ m_{23}=m_c sin\theta,\ \ m_{25}=m_{52}=m_c l cos\theta,$$

$$m_{32}=m_c sin\theta,\ \ m_{33}=m_l+m_c,\ \ m_{44}=m_c l^2 cos^2\theta,\ \ m_{55}=m_c l^2.$$

The coefficients of the $\mathbf{C}(\mathbf{q},\dot{\mathbf{q}})$ matrix are determined by the following equations:

$$c_{13}=m_c cos\varphi cos\theta\dot{\varphi}-m_c sin\varphi sin\theta\dot{\theta},$$

$$c_{14}=m_c cos\varphi cos\theta\dot{l}-m_c l cos\varphi sin\theta\dot{\theta}-m_c l sin\varphi cos\theta\dot{\varphi},$$

$$c_{15}=-m_c l cos\varphi sin\theta\dot{\varphi}-m_c sin\varphi sin\theta\dot{l}-m_c l sin\varphi cos\theta\dot{\theta},$$

$$c_{23}=m_c cos\theta\dot{\theta},\ \ c_{25}=m_c cos\theta\dot{l}-m_c l sin\theta\dot{\theta},$$

$$c_{34}=-m_c l cos^2\theta\dot{\varphi},\ \ c_{35}=-m_c l\dot{\theta},\ \ c_{43}=m_c l cos^2\theta\dot{\varphi},$$

$$c_{44}=m_c l cos^2\theta\dot{l}-m_c l^2 cos\theta sin\theta\dot{\theta},\ \ c_{45}=-m_c l^2 cos\theta sin\theta\dot{\varphi},$$

$$c_{53}=m_c l\dot{\theta},\ \ c_{54}=m_c l^2 cos\theta sin\theta\dot{\varphi},\ \ c_{55}=m_c l\dot{l}.$$

The nonzero coefficients of the $\mathbf{G}(\mathbf{q})$ vector are determined by the following equations:

$$g_3=-m_c g cos\varphi cos\theta,\ \ g_4=m_c g l sin\varphi cos\theta,\ \ g_5=m_c g l cos\varphi sin\theta.$$

3. Second-Order Sliding Mode Controller

3.1 Decoupling

An overhead crane is an under-actuated system with five controlled outputs but only three actuators. The mathematical model for the overhead crane should be separated into two auxiliary dynamic models comprising actuated and un-actuated systems. Correspondingly, we define $\mathbf{q}_1=[z\ \ x\ \ l]^T$ for actuated states and $\mathbf{q}_2=[\varphi\ \ \theta]^T$ for un-actuated states. The matrix shown in Eq. (6) can be separated into two equations:

$$\begin{Bmatrix} \mathbf{M}_{11}(\mathbf{q})\ddot{\mathbf{q}}_a+\mathbf{M}_{12}(\mathbf{q})\ddot{\mathbf{q}}_u+\mathbf{B}_{11}\dot{\mathbf{q}}_a \\ +\mathbf{C}_{11}(\mathbf{q},\dot{\mathbf{q}})\dot{\mathbf{q}}_a+\mathbf{C}_{12}(\mathbf{q},\dot{\mathbf{q}})\dot{\mathbf{q}}_u+\mathbf{G}_1(\mathbf{q}) \end{Bmatrix}=\mathbf{U}, \tag{7}$$

$$\begin{Bmatrix} \mathbf{M}_{21}(\mathbf{q})\ddot{\mathbf{q}}_a+\mathbf{M}_{22}(\mathbf{q})\ddot{\mathbf{q}}_u+\mathbf{C}_{21}(\mathbf{q},\dot{\mathbf{q}})\dot{\mathbf{q}}_a \\ +\mathbf{C}_{22}(\mathbf{q},\dot{\mathbf{q}})\dot{\mathbf{q}}_u+\mathrm{G}_2(\mathbf{q})) \end{Bmatrix}=0, \tag{8}$$

where

$$\mathbf{M}_{11}(\mathbf{q})=\begin{bmatrix} m_{11} & 0 & m_{13} \\ 0 & m_{22} & m_{23} \\ m_{31} & m_{32} & m_{33} \end{bmatrix},\ \mathbf{M}_{12}(\mathbf{q})=\begin{bmatrix} m_{14} & m_{15} \\ 0 & m_{25} \\ 0 & 0 \end{bmatrix},$$

$$\mathbf{M}_{21}(\mathbf{q})=\begin{bmatrix} m_{41} & 0 & 0 \\ m_{51} & m_{52} & 0 \end{bmatrix},\ \mathbf{M}_{22}(\mathbf{q})=\begin{bmatrix} m_{44} & 0 \\ 0 & m_{55} \end{bmatrix},$$

$$\mathbf{C}_{11}(\mathbf{q},\dot{\mathbf{q}})=\begin{bmatrix} 0 & 0 & c_{13} \\ 0 & 0 & c_{23} \\ 0 & 0 & 0 \end{bmatrix},\ \mathbf{C}_{12}(\mathbf{q},\dot{\mathbf{q}})=\begin{bmatrix} c_{14} & c_{15} \\ 0 & c_{25} \\ c_{34} & c_{35} \end{bmatrix},$$

$$\mathbf{C}_{21}(\mathbf{q},\dot{\mathbf{q}})=\begin{bmatrix} 0 & 0 & c_{43} \\ 0 & 0 & c_{53} \end{bmatrix},\ \mathbf{C}_{22}(\mathbf{q},\dot{\mathbf{q}})=\begin{bmatrix} c_{44} & c_{45} \\ c_{54} & c_{55} \end{bmatrix},$$

$$\mathbf{B}_{11}=\begin{bmatrix} b_b & 0 & 0 \\ 0 & b_t & 0 \\ 0 & 0 & b_l \end{bmatrix},\ \mathbf{G}_1=\begin{bmatrix} 0 \\ 0 \\ g_3 \end{bmatrix},\ \mathbf{G}_2=\begin{bmatrix} g_4 \\ g_5 \end{bmatrix},\ \mathbf{U}=\begin{bmatrix} u_b \\ u_t \\ u_l \end{bmatrix}.$$

$\mathbf{M}_{22}(\mathbf{q})$ is a positive definite matrix. Eq. (8) is rewritten as follows:

$$\ddot{\mathbf{q}}_u=-\mathbf{M}_{22}^{-1}(\mathbf{q})\begin{Bmatrix} \mathbf{M}_{21}(\mathbf{q})\ddot{\mathbf{q}}_a+\mathbf{C}_{21}(\mathbf{q},\dot{\mathbf{q}})\dot{\mathbf{q}}_a \\ +\mathbf{C}_{22}(\mathbf{q},\dot{\mathbf{q}})\dot{\mathbf{q}}_u+\mathbf{G}_2(\mathbf{q}) \end{Bmatrix}. \tag{9}$$

Cargo swing $\mathbf{q}_2=[\varphi\ \ \theta]^T$ is directly involved in the properties of trolley motion x, bridge motion z, and cable length l. Substituting Eq. (9) with Eq. (7) and simplifying the lead to the actuated dynamics derive the following equation:

$$\overline{\mathbf{M}}(\mathbf{q})\ddot{\mathbf{q}}_a+\overline{\mathbf{C}}_1(\mathbf{q},\dot{\mathbf{q}})\dot{\mathbf{q}}_a+\overline{\mathbf{C}}_2(\mathbf{q},\dot{\mathbf{q}})\dot{\mathbf{q}}_u+\overline{\mathbf{G}}(\mathbf{q})=\mathbf{U}, \tag{10}$$

where

$$\overline{\mathbf{M}}(\mathbf{q})=\mathbf{M}_{11}(\mathbf{q})-\mathbf{M}_{12}(\mathbf{q})\mathbf{M}_{22}^{-1}(\mathbf{q})\mathbf{M}_{21}(\mathbf{q}),$$

$$\overline{\mathbf{C}}_1(\mathbf{q},\dot{\mathbf{q}})=\mathbf{B}_{11}+\mathbf{C}_{11}(\mathbf{q},\dot{\mathbf{q}})-\mathbf{M}_{12}(\mathbf{q})\mathbf{M}_{22}^{-1}(\mathbf{q})\mathbf{C}_{21}(\mathbf{q},\dot{\mathbf{q}}),$$

$$\overline{\mathbf{C}}_2(\mathbf{q},\dot{\mathbf{q}})=\mathbf{C}_{12}(\mathbf{q},\dot{\mathbf{q}})-\mathbf{M}_{12}(\mathbf{q})\mathbf{M}_{22}^{-1}(\mathbf{q})\mathbf{C}_{22}(\mathbf{q},\dot{\mathbf{q}}),$$

$$\overline{\mathbf{G}}(\mathbf{q})=\mathbf{G}_1(\mathbf{q})-\mathbf{M}_{12}(\mathbf{q})\mathbf{M}_{22}^{-1}(\mathbf{q})\mathbf{G}_2(\mathbf{q}).$$

3.2 Control scheme design

A second-order sliding mode controller is proposed to move the trolley and the bridge from their initial positions to their destinations as fast as possible, to reduce cargo vibrations during transfer, and to eliminate cargo swings at the trolley and bridge destinations. All the state variables are assumed to be measurable. The SMC algorithm design has two phases. First, the sliding surface is selected to consolidate all state trajectories. Second, the SMC scheme is designed to push all system states to the reference points on the sliding surface. In other words, under the action of the proposed controller, the actuated states $\mathbf{q}_1=[z\ \ x\ \ l]^T$ reach the desired values $\mathbf{q}_{1d}=[z_d\ \ x_d\ \ l_d]^T$ and the cargo swings $\mathbf{q}_2=[\varphi\ \ \theta]^T$ converge to $\mathbf{q}_{2d}=[0\ \ 0]^T$.

The first-order sliding surface is defined as

$$\mathbf{s} = [s_1 \quad s_2 \quad s_3]^T = \dot{\tilde{\mathbf{q}}}_1 + \lambda\tilde{\mathbf{q}}_1 + \alpha\tilde{\mathbf{q}}_2 , \tag{11}$$

where $\lambda = \begin{bmatrix} \lambda_1 & 0 & 0 \\ 0 & \lambda_2 & 0 \\ 0 & 0 & \lambda_3 \end{bmatrix}$ and $\alpha = \begin{bmatrix} \alpha_1 & 0 \\ 0 & \alpha_2 \\ 0 & 0 \end{bmatrix}$ are design parameters, and $\tilde{\mathbf{q}}_1 = \mathbf{q}_1 - \mathbf{q}_{1d} = [z_b - z_d \;\; x_t - x_d \;\; l - l_d]^T$ and $\tilde{\mathbf{q}}_2 = \mathbf{q}_2 - \mathbf{q}_{2d} = [\varphi \;\; \theta]^T$ are tracking error vectors.

By differentiating the sliding surface with respect to time, we obtain the following equation:

$$\mathbf{s} = \ddot{\tilde{\mathbf{q}}}_1 + \lambda\dot{\tilde{\mathbf{q}}}_1 + \alpha\dot{\tilde{\mathbf{q}}}_2 \tag{12}$$

which leads to

$$\dot{\mathbf{s}} = \ddot{\mathbf{q}}_1 + \lambda\dot{\mathbf{q}}_1 + \alpha\dot{\mathbf{q}}_2 . \tag{13}$$

We consider the surface dynamics, expressed as follows:

$$\dot{\mathbf{s}} + \lambda\mathbf{s} = 0 . \tag{14}$$

Eq. (14) indicates that the sliding surface **s** is exponentially stable for every positive diagonal matrix λ. By inserting Eq. (10) into Eq. (13) and Eqs. (11) and (13) into Eq. (14), we obtain the following equivalent control input:

$$\begin{aligned} \mathbf{U}_{eq} &= \overline{\mathbf{C}}_1(\mathbf{q},\dot{\mathbf{q}})\dot{\mathbf{q}}_1 + \overline{\mathbf{C}}_2(\mathbf{q},\dot{\mathbf{q}})\dot{\mathbf{q}}_2 + \overline{\mathbf{G}}(\mathbf{q}) \\ &\quad - \overline{\mathbf{M}}(\mathbf{q})\{2\lambda\dot{\mathbf{q}}_1 + \lambda^T\lambda(\mathbf{q}_1 - \mathbf{q}_{1d}) + \alpha\dot{\mathbf{q}}_2 + \lambda\alpha\mathbf{q}_2\} . \end{aligned} \tag{15}$$

The equivalent component shown in Eq. (15) consolidates the system states toward the sliding surface. To consistently maintain system trajectories on the sliding surface, we introduce the switching action, expressed as follows:

$$\mathbf{U}_{sw} = -\mathbf{K}\mathbf{sgn}(\mathbf{s}) . \tag{16}$$

The second-order SMC scheme, which comprises approximated action and switching control, now becomes

$$\begin{aligned} \mathbf{U} &= \overline{\mathbf{C}}_1(\mathbf{q},\dot{\mathbf{q}})\dot{\mathbf{q}}_1 + \overline{\mathbf{C}}_2(\mathbf{q},\dot{\mathbf{q}})\dot{\mathbf{q}}_2 + \overline{\mathbf{G}}(\mathbf{q}) - \mathbf{K}\mathbf{sgn}(\mathbf{s}) \\ &\quad - \overline{\mathbf{M}}(\mathbf{q})\{2\lambda\dot{\mathbf{q}}_1 + \lambda^T\lambda(\mathbf{q}_1 - \mathbf{q}_{1d}) + \alpha\dot{\mathbf{q}}_2 + \lambda\alpha\mathbf{q}_2\} , \end{aligned} \tag{17}$$

where $\mathbf{K} = \mathrm{diag}(K_1, K_2, K_3)$ Controller parameters **K**, **l**, and **a** are also chosen to stabilize the sliding surface and to enable the state trajectories to slide to the desired values on surface **s** as fast as possible. The sign function of the sliding surface is denoted by **sgn**(s).

3.3 Stability of sliding surface

The ability of the second-order sliding mode controller, shown in Eq. (17), to asymptotically stabilize the sliding surface defined by Eq. (11) should be proven. The following Lyapunov positive candidate is considered:

$$V = \frac{1}{2}\mathbf{s}^T\mathbf{s} \tag{18}$$

with a derivative in of the form of

$$\dot{V} = \dot{\mathbf{s}}^T\mathbf{s} . \tag{19}$$

Notably, $\overline{\mathbf{M}}(\mathbf{q})$ is a positive definite matrix. The actuated dynamics shown in Eq. (10) is rewritten as follows:

Table 1 Crane parameters

System parameters	Controller parameters
g = 9.81 m/s^2; m_c = 0.85 kg m_t = 5 kg; m_b = 7 kg m_l = 2 kg; b_t = 20 Nm/s b_b = 30 Nm/s; b_r = 50 Nm/s	λ = diag (0.75, 0.75, 1) α_1 = 4; α_2 = 3.5 **K** = diag (0.5, 0.5, 1)

$$\ddot{\mathbf{q}}_1 = \overline{\mathbf{M}}^{-1}(\mathbf{q})\{\mathbf{U} - \overline{\mathbf{C}}_1(\mathbf{q},\dot{\mathbf{q}})\dot{\mathbf{q}}_1 - \overline{\mathbf{C}}_2(\mathbf{q},\dot{\mathbf{q}})\dot{\mathbf{q}}_2 - \overline{\mathbf{G}}(\mathbf{q})\} . \tag{20}$$

Substituting Eq. (17) with Eq. (20) and Eq. (20) with Eq. (19) yields the following equation:

$$\dot{V} = -\mathbf{s}^T\lambda\mathbf{s} - \mathbf{s}^T\overline{\mathbf{M}}^{-1}(\mathbf{q})\mathbf{K}\mathbf{sgn}(\mathbf{s}) . \tag{21}$$

The sign of s_i is identical to that of sgn(s_i). Therefore, the sign consideration of $\dot{V}$ is equivalent to that of the following function:

$$V_1 = -\mathbf{s}^T\lambda\mathbf{s} - \mathbf{s}^T\overline{\mathbf{M}}^{-1}(\mathbf{q})\mathbf{K}\mathbf{s} . \tag{22}$$

After some calculations, $\overline{\mathbf{M}}(\mathbf{q})$ is derived in the following form:

$$\overline{\mathbf{M}}(\mathbf{q}) = \begin{bmatrix} \begin{pmatrix} m_t + m_b + m_c \\ sin^2\varphi\, cos^2\theta \end{pmatrix} & \begin{pmatrix} m_c sin\varphi \\ sin\theta cos\theta \end{pmatrix} & (m_c sin\varphi cos\theta) \\ \begin{pmatrix} m_c sin\varphi \\ sin\theta cos\theta \end{pmatrix} & \begin{pmatrix} m_t + m_c \\ sin^2\theta \end{pmatrix} & (m_c sin\theta) \\ (m_c sin\varphi cos\theta) & (m_c sin\theta) & (m_l + m_c) \end{bmatrix} . \tag{23}$$

$\overline{\mathbf{M}}(\mathbf{q})$ is a symmetric matrix with $a_{11} = m_t + m_b + m_c\sin^2\varphi\cos^2\theta > 0$. The determinants of the upper-left sub-matrices of $\overline{\mathbf{M}}(\mathbf{q})$ are

$$\det(\overline{\mathbf{M}}_1(\mathbf{q})) = \begin{Bmatrix} m_t^2 + m_t m_b + m_t m_c sin^2\varphi\, cos^2\theta \\ +(m_t m_c + m_b m_c) sin^2\theta \end{Bmatrix} > 0$$

and

$$\det(\overline{\mathbf{M}}(\mathbf{q})) = \begin{Bmatrix} m_t(m_t + m_c)(m_t + m_b) \\ +m_c m_l(m_t + m_b) sin^2\theta \\ +m_t m_c m_l sin^2\varphi\, cos^2\theta \end{Bmatrix} > 0 .$$

Therefore, $\overline{\mathbf{M}}(\mathbf{q})$ is a positive definite matrix for every **q**.

Eq. (22) shows that $V_1 \le 0$ for every positive definite matrix $\overline{\mathbf{M}}(\mathbf{q})$ and controller gains $\mathbf{K} > 0$ and $\lambda > 0$, yielding $\dot{V} \le 0$, which implies $V(t) \le V(0)$. Therefore, **s** must be bounded. We apply Barbalat's lemma,[39] $\lim_{t\to\infty} \dot{V} = 0$, which yields $\lim_{t\to\infty} \mathbf{s} = 0$. Hence, the sliding surface **s** is asymptotically stable.

4. Simulation and Experiment

The system dynamics shown in Eqs. (7) and (8), and obtained by using the second-order SMC input shown in Eq. (17) is numerically simulated via MATLAB. The simulation is implemented for the most complicated case in which all crane mechanisms are simultaneously operated. More precisely, the cargo is lifted from the 1 m initial cable

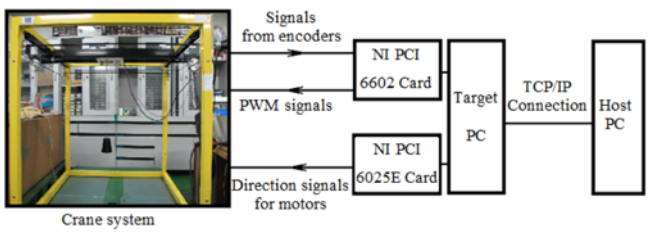

Fig. 2 Diagram structure of a real-time crane system

length to the 0.7 m desired cable length. The trolley is driven to move from its initial position to the 0.4 m desired displacement. The bridge is controlled to move to the 0.3 m reference. The suspended cargo cable is initially perpendicular to the ground ($\varphi_0 = \theta_0 = 0^0$). The crane system is simulated by using the two cases described in the following paragraphs.

Case 1: The crane parameters used in this case are shown in Table 1.

Case 2: System with uncertainties. Several crane parameters have uncertainties that can be extensively varied depending on operating conditions. Overhead cranes hoist cargo of varying volumes and weights. The friction factors can be changed in connection with temperature and operating environment. Therefore, the proposed controller must guarantee system robustness in case of system parameter variation. Using the controller parameters in Case 1, the system responses are investigated when the cargo mass m_c = 400% is increased (m_c = 3.4 kg) and when the damped coefficients $\Delta b_t = \Delta b_b = \Delta b_r$ = -10% are decreased (b_t = 18 Nm/s, b_b = 27 Nm/s, and b_r = 45 Nm/s).

Experiments were conducted on a laboratory overhead crane (Fig. 2), and the results were compared with the simulation results. The crane system comprises two IG32GM direct current (DC) geared motors for driving the trolley and hoisting the cargo. Three HEDM 5505 incremental encoders manufactured by Hewlett-Packard, with resolutions of up to 1,024 counts per revolution, were used to measure trolley displacement, cable length, and payload swing angle. The crane system was controlled in real time by a host personal computer (PC) with MATLAB and SIMULINK environments by using the xPC Target solution. The target PC is equipped with two additional interface cards to achieve the proposed control. The first interface card is the NI PCI 6025E multifunction card, which is used to send directional control commands to the motor amplifiers. The other card is the NI PCI 6602 card, which acquires pulse signals from the encoders and sends pulse width modulation signals to the amplifiers. The real-time crane system was operated at a sampling time of $T_s = 10^3$ s.

The results are shown in Figs. 3 to 15. The high quality of the bridge, trolley, and cargo-hoisting motions are shown in Figs. 3 to 5. These responses have no overshoot and converge to a steady state after a considerably short time. For example, the trolley moves to the 0.4 m desired position after 5.6 s for simulation Case 1 and 4.4 s for the experiment. The cargo is lifted to the 0.7 m desired cable length from the 1 m initial position after 5.5 s for simulation Case 1 and 3.8 s for the experiment. The shapes of transient responses were consistently retained when the system parameters m_c, b_b, b_t, and b_r were broadly modified (the dot curves denote uncertainties).

The payload swings for the simulation and experiment are shown in Figs. 6 and 7 respectively. The experimental cargo swings of this study

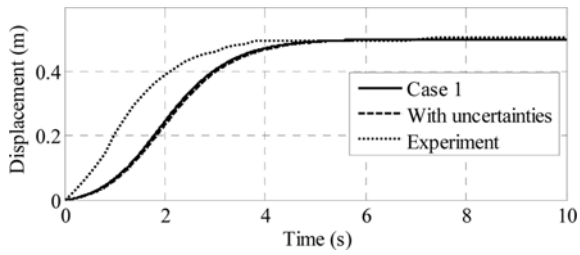

Fig. 3 Bridge motion

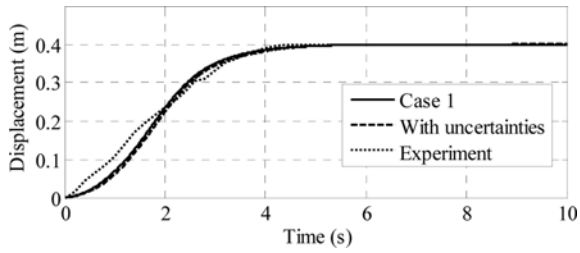

Fig. 4 Trolley motion

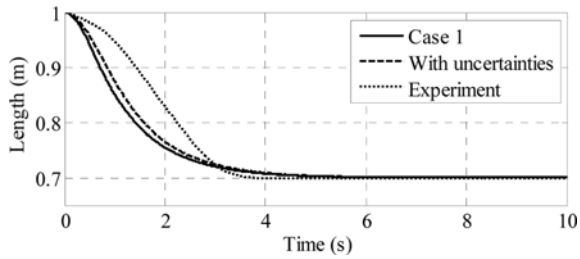

Fig. 5 Cable length

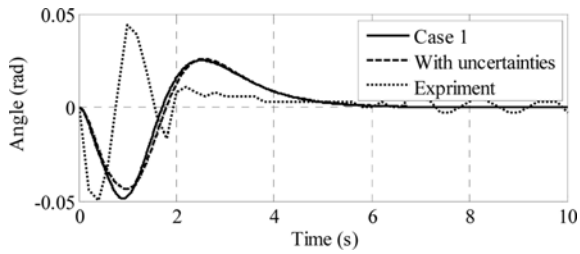

Fig. 6 Cargo swing, φ

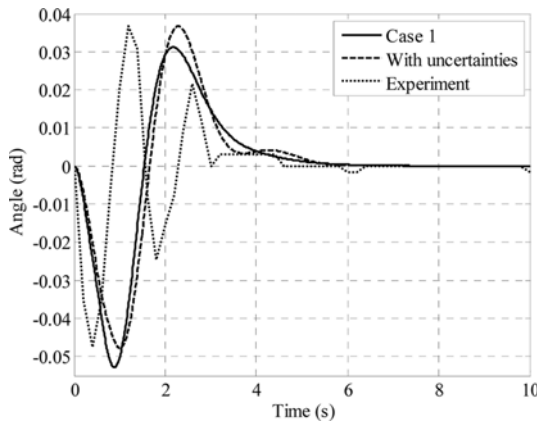

Fig. 7 Cargo swing, θ

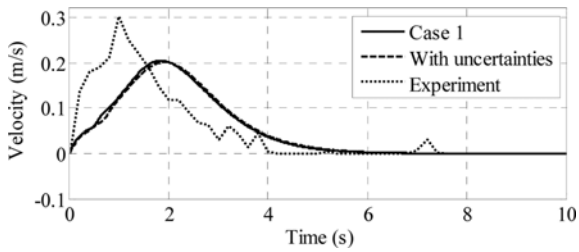

Fig. 8 Bridge velocity

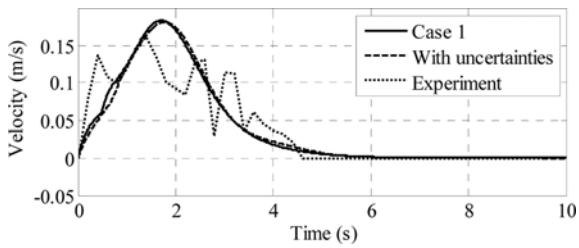

Fig. 9 Trolley velocity

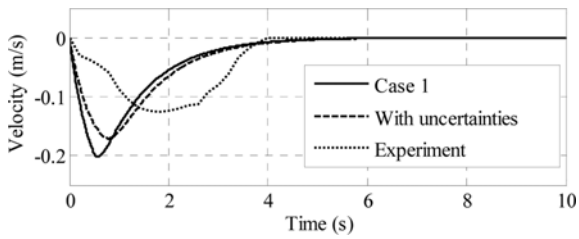

Fig. 10 Cargo-hoisting velocity

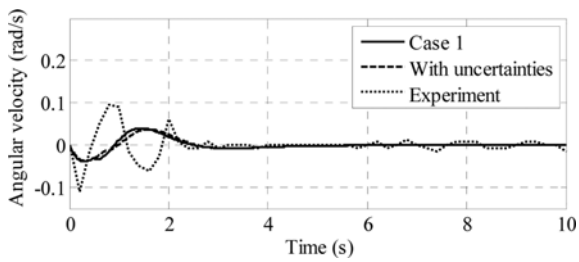

Fig. 11 Cargo swing velocity, $\dot{\varphi}$

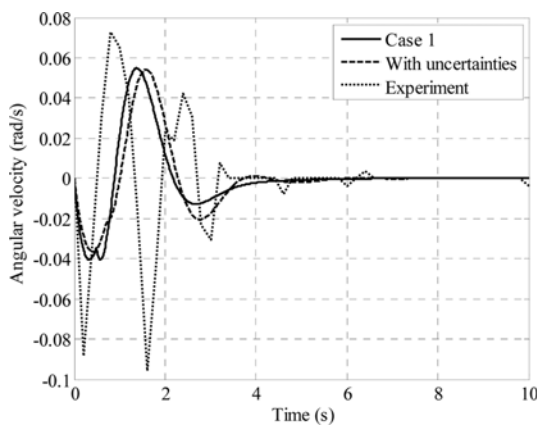

Fig. 12 Cargo swing velocity, $\dot{\theta}$

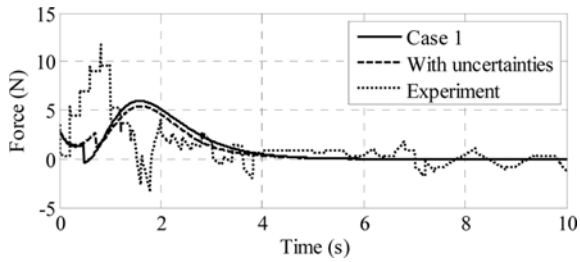

Fig. 13 Bridge-moving force

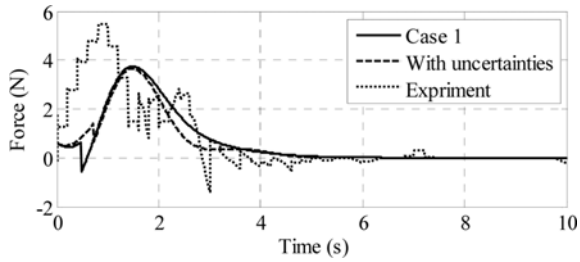

Fig. 14 Trolley-driving force

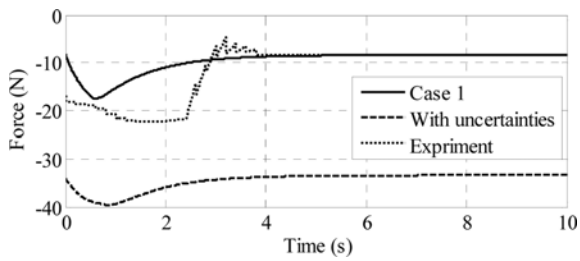

Fig. 15 Payload-lifting force

are comparatively smooth. A small payload was maintained during the transfer process: $\varphi_{max} = 2.7^o$ for the simulation and $\varphi_{max} = 2.9^o$ for the experiment; $\theta_{max} = 3^o$ for the simulation and $\theta_{max} = 2.7^o$ for the experiment. Cargo swings were suppressed within one vibration cycle for the simulation and more than two cycles for the experiment. The amount of time needed by the cargo vibration curves to achieve the steady state differs between the simulation and the experiment: $t_s = 7$ s for j-simulation and $t_s = 6$ s for j-experiment; $t_s = 5.7$ s for q-simulation and $t_s = 6.4$ s for q-experiment. The q-steady experiment response vanished, whereas the j-experiment response remained at steady-state error $e_{ss} = 0.32^o$.

In practice, overhead cranes are not equipped with velocity sensors because of increases in cost, weight, and volume of cranes. Velocities can be obtained by deriving the displacements or estimating the states using an observer. In this study, numerical derivation was used to obtain the velocities. The velocities of system responses are depicted in Figs. 8 to 12. The transient periods of simulated velocities of the bridge, trolley, and lifted cargo are divided into the accelerating and decelerating phases. For example, the bridge speeds up in the first 1.9 s and slows down in the remaining 4.3 s. The trolley accelerates in the first 1.8 s and decelerates in the remaining 3.8 s. Cargo is hoisted with high speed in the first 0.6 s and with low speed in the remaining 4.9 s. The peaks of these responses show the transition stages between the two phases.

Table 2 Comparison of experimental performance with Bartolini's research[36]

	Settling time (s)		M_p (%) or a_{max} (rad)		Steady-state error	
	Our study		Our study		Our study	
z (m)	4	X	0	X	0.004 m	X
x (m)	4.4	7	0	0	0	0
l (m)	3.8	6	0	0	0	0
φ (rad)	5.6	X	0.050 rad	X	0.006 rad	X
θ (rad)	4.6	8	0.048 rad	0.13 rad	0.0015 rad	0.02 rad

"X" denotes that the "value is not available."

M_p and a_{max} denote the "maximum percentage overshoot" and "maximum swing angle," respectively.

Table 3 Comparison of simulation performance with Almutairi's research[38]

	Settling time (s)		M_p (%) or a_{max} (rad)		Steady-state error	
	Our study		Our study		Our study	
z (m)	6.8	14	0	5%	0	0
x (m)	6.8	15	0	6%	0	0
l (m)	6.5	8	0	0%	0	0
φ (rad)	6.9	16	0.049 rad	2.9 rad	0	0
θ (rad)	7.6	14	0.053 rad	2.3 rad	0	0

M_p and a_{max} denote the "maximum percentage overshoot" and "maximum swing angle," respectively.

The responses of bridge and trolley motions have smooth transition stages, whereas the response of cargo hoisting has a sudden transition stage.

The system responses described in Figs. 3 to 15 point out the difference between simulation and experimental curves, and are obviously seen at the transient state. This result is derived from the discrepancy between the mathematical model and the real crane system. Several nonlinearities and factors were not included in the mathematical model, such as nonlinear frictions and precise modeling of DC motors. Certainly, if the mathematical model becomes consistent with the real crane system, then the simulation results will eventually become similar to the experiment results.

Table 2 further shows the strength of the proposed controller by comparing the experimental results between our study and Bartolini's research.[36] Three performance indices for the time response of bridge motion, trolley motion, payload hoisting, and two directional cargo swing angles φ and θ are compared. Considering that Bartolini studied the second-order sliding mode controller that was designed only for 2D motion, no performance measure was obtained for bridge motion and cargo swing angle φ, and they are denoted with "X" in Table 2. A comparison shows that the response of our study is faster than that of Bartolini's research. The maximum value and the steady-state error of the swing angle of our result are also far smaller than those of Bartolini. Unlike the experimental swing angle in Bartolini's research, wherein the cargo vibrated with more than four cycles and the chattering was clearly observable, the experimental cargo swings in the current study are smooth. Although our study handles the 3D motion of an overhead crane, which is more difficult to control than the 2D case, all three performance indices denote that our controller is much better than that in Bartolini's research.

A comparison with the research of Almutairi[38] is shown in Table 3. Almutairi proposed a first-order sliding mode controller for a 3D overhead crane, but he investigated only the simulation and presented the simulation result for his proposed controller. While the bridge and trolley motions of Almutairi's research clearly have significant overshoots, the bridge, trolley, and cargo-hoisting motions of our study have no overshoot and converge to a steady state after a considerably short time.

5. Conclusion

A second-order sliding mode nonlinear controller was improved for a 3D crane system in a complicated operation in which cargo lifting, trolley traveling, and bridge moving were simultaneously activated. Simulations and experiments were performed. Most of system responses were asymptotically stabilized. The experimental payload swings approximately approached zero in spite of a small residual steady-state error. The bridge and trolley motions approached reference input values without maximum overshoots. The controller guarantees system robustness despite the extensive variety of system parameters. The optimal SMC of overhead cranes will be enhanced in future work.

ACKNOWLEDGMENT

This research was partially supported by the Ministry of Trade, Industry and Energy (MOTIE) of South Korea with supervision from the Korea Evaluation Institute of Industrial Technology (KEIT) (Grant No. 10041629, Implementation of Technologies for Identification, Behavior, and Location of Human based on Sensor Network Fusion Program), as well as the Technology Innovation Program (10040992) of MOTIE/KEIT. Also, this research was supported by a grant of the Technology Innovation Program of the Knowledge economy of MKE (No. 10041834, Technology development of service robot's performance and standardization for movement/manipulation/HRI/networking).

REFERENCES

1. Sakawa, Y. and Sano, H., "Nonlinear Model and Linear Robust Control of Overhead Traveling Cranes," Nonlinear Analysis: Theory, Methods & Applications, Vol. 30, No. 4, pp. 2197-2207, 1997.
2. Sawodny, O., Aschemann, H., and Lahres, S., "An Automated Gantry Crane as a Large Workspace Robot," Control Engineering Practice, Vol. 10, No. 12, pp. 1323-1338, 2002.
3. Giua, A., Seatzu, C., and Usai, G., "Observer-Controller Design for Cranes Via Lyapunov Equivalence," Automatica, Vol. 35, No. 4, pp. 669-678, 1999.
4. Sakawa, Y. and Shindo, Y., "Optimal Control of Container Cranes," Automatica, Vol. 18, No. 3, pp. 257-266, 1982.
5. Auernig, J. and Troger, H., "Time Optimal Control of Overhead Cranes with Hoisting of the Load," Automatica, Vol. 23, No. 4, pp. 437-447, 1987.

6. Al-Garni, A. Z., Moustafa, K. A. F., and Javeed Nizami, S., "Optimal Control of Overhead Cranes," Control Engineering Practice, Vol. 3, No. 9, pp. 1277-1284, 1995.

7. Wang, Z. and Surgenor, B. W., "A Problem with the LQ Control of Overhead Cranes," Journal of Dynamic Systems, Measurement, and Control, Vol. 128, No. 2, pp. 436-440, 2006.

8. Park, H., Chwa, D., and Hong, K., "A Feedback Linearization Control of Container Cranes: Varying Rope Length," International Journal of Control Automation and Systems, Vol. 5, No. 4, pp. 379-387, 2007.

9. Le, T. A., Kim, G. H., Kim, M. Y., and Lee, S. G., "Partial Feedback Linearization Control of Overhead Cranes with Varying Cable Lengths," Int. J. Precis. Eng. Manuf., Vol. 13, No. 4, pp. 501-507, 2012.

10. Cheng, C. C. and Chen, C. Y., "Controller Design for an Overhead Crane System with Uncretainty," Control Engineering Practice, Vol. 4, No. 5, pp. 645-653, 1996.

11. Cho, H. C., Lee, J. W., Lee, Y. J., and Lee, K. S., "Lyapunov Theory based Robust Control of Complicated Nonlinear Mechanical Systems with Uncertainty," Journal of Mechanical Science and Technology, Vol. 22, No. 11, pp. 2142-2150, 2008.

12. Kim, C. S. and Hong, K. S., "Boundary Control of Container Cranes from the Perspective of Controlling an Axially Moving String System," International Journal of Control, Automation and Systems, Vol. 7, No. 3, pp. 437-445, 2009.

13. Kim, Y. S., Hong, K. S., and Sul, S. K., "Anti-Sway Control of Container Cranes: Inclinometer, Observer, and State Feedback," International Journal of Control, Automation, and Systems, Vol. 2, No. 4, pp. 435-449, 2004.

14. Fang, Y., Dixon, W. E., Dawson, D. M., and Zergeroglu, E., "Non-linear Coupling Control Laws for an Enderactuated Overhead Crane System," IEEE/ASME Transactions on Mechatronics, Vol. 8, No. 3, pp. 418-423, 2003.

15. Chwa, D., "Nonlinear Tracking Control of 3-D Overhead Cranes Against the Initial Swing Angle and the Variation of Payload Weight," IEEE Transactions on Control Systems Technology, Vol. 17, No. 4, pp. 876-883, 2009.

16. Moustafa, K. A., "Reference Trajectory Tracking of Overhead Cranes," Journal of Dynamic Systems, Measurement, and Control, Vol. 123, No. 1, pp. 139-141, 2001.

17. Lee, H. H., "A New Approach for the Anti-Swing Control of Overhead Cranes with High-Speed Load Hoisting," International Journal of Control, Vol. 76, No. 15, pp. 1493-1499, 2003.

18. Lee, H. H., "A New Motion-Planning Scheme for Overhead Cranes with High-Speed Hoisting," Journal of Dynamic Systems, Measurement, and Control, Vol. 126, No. 2, pp. 359-364, 2004.

19. Lee, H. H., "Motion Planning for Three-Dimensional Overhead Cranes with High-Speed Load Hoisting," International Journal of Control, Vol. 78, No. 12, pp. 875-886, 2005.

20. Yang, J. H. and Yang, K. S., "Adaptive Coupling Control for Overhead Crane Systems," Mechatronics, Vol. 17, No. 2, pp. 143-152, 2007.

21. Yang, J. H. and Shen, S. H., "Novel Approach for Adaptive Tracking Control of a 3-D Overhead Crane System," Journal of Intelligent & Robotic Systems, Vol. 62, No. 1, pp. 59-80, 2011.

22. Teo, C. S., Tan, K. K., Lim, S. Y., Huang, S., and Tay, E. B., "Dynamic Modeling and Adaptive Control of a H-Type Gantry Stage," Mechatronics, Vol. 17, No. 7, pp. 361-367, 2007.

23. Cho, H. C. and Lee, K. S., "Adaptive Control and Stability Analysis of Nonlinear Crane Systems with Perturbation," Journal of Mechanical Science and Technology, Vol. 22, No. 6, pp. 1091-1098, 2008.

24. Sun, N., Fang, Y., Zhang, Y., and Ma, B., "A Novel Kinematic Coupling-based Trajectory Planning Method for Overhead Cranes," IEEE/ASME Transactions on Mechatronics, Vol. 17, No. 1, pp. 166-173, 2012.

25. Omar, H. M. and Nayfeh, A. H., "Gain Scheduling Feedback Control for Tower Cranes," Journal of Vibration and Control, Vol. 9, No. 3-4, pp. 399-418, 2003.

26. Giua, A., Sanna, M., and Seatzu, C., "Observer-Controller Design for Three Dimensional Overhead Cranes using Time-Scaling," Mathematical and Computer Modelling of Dynamical Systems, Vol. 7, No. 1, pp. 77-107, 2001.

27. Corriga, G., Giua, A., and Usai, G., "An Implicit Gain-Scheduling Controller for Cranes," IEEE Transactions on Control Systems Technology, Vol. 6, No. 1, pp. 15-20, 1998.

28. Mizumoto, I., Chen, T., Ohdaira, S., Kumon, M., and Iwai, Z., "Adaptive Output Feedback Control of General MIMO Systems using Multirate Sampling and its Application to a Cart-Crane System," Automatica, Vol. 43, No. 12, pp. 2077-2085, 2007.

29. Ngo, Q. H., Hong, K. S., and Jung, I. H., "Adaptive Control of an Axially Moving System," Journal of Mechanical Science and Technology, Vol. 23, No. 11, pp. 3071-3078, 2009.

30. Lee, K., Coate, S., and Carroll, V. C., "Variable Structure Control Applied to Underactuated Robots," Robotica, Vol. 15, No. 3, pp. 313-318, 1997.

31. Ashrafiuon, H. and Erwin, R. S., "Sliding Mode Control of Underactuated Multibody Systems and its Application to Shape Change Control," International Journal of Control, Vol. 81, No. 12, pp. 1849-1858, 2008.

32. Sankaranarayanan, V. and Mahindrakar, A.D., "Control of a Class of Underactuated Mechanical Systems Using Sliding Modes," IEEE Transactions on Robotics, Vol. 25, No. 2, pp. 459-467, 2009.

33. Karkoub, M. A. and Zribi, M., "Robust Control Schemes for an Overhead Crane," Journal of Vibration and Control, Vol. 7, No. 3, pp. 395-416, 2001.

34. Bartolini, G., Pisano, A., and Usai, E., "Output-Feedback Control of container Cranes: A Comparative Analysis," Asian Journal of Control, Vol. 5, no. 4, pp. 578-593, 2003.

35. Ngo, Q. H. and Hong, K. S., "Sliding-Mode Antisway Control of an Offshore Container Crane," IEEE/ASME Transactions on Mechatronics, Vol. 17, No. 2, pp. 201-209, 2012.

36. Bartolini, G., Pisano, A., and Usai, E., "Second-Order Sliding-Mode Control of Container Cranes," Automatica, Vol. 38, No. 10, pp. 1783-1790, 2002.

37. Lee, H. H., Liang, Y., and Segura, D., "A Sliding-Mode Antiswing Trajectory Control for Overhead Cranes with High-Speed Load Hoisting," Journal of Dynamic Systems, Measurement, and Control, Vol. 128, No. 4, pp. 842-845, 2006.

38. Almutairi, N. B. and Zribi, M., "Sliding Mode Control of a Three-Dimensional Overhead Crane," Journal of Vibration and Control, Vol. 15, No. 11, pp. 1679-1730, 2009.

39. Slotine, J. J. E. and Li, W., "Applied Nonlinear Control," Prentice Hall, pp. 123, 1991.